

Microfibril Angles Inside and Outside Crossfields of Norway Spruce Tracheids

By Helga C. Lichtenegger^{1,2}, Martin Müller^{3,4}, Rupert Wimmer⁵ and Peter Fratzl¹

¹ Erich Schmid Institute for Materials Science, Austrian Academy of Sciences and University of Leoben, Leoben, Austria

² Department of Chemistry and Biochemistry, University of California Santa Barbara, USA

³ European Synchrotron Radiation Facility, (ESRF), Grenoble, France

⁴ Institute for Experimental and Applied Physics, University of Kiel, Germany

⁵ Institute for Botany, University for Agricultural Sciences, Vienna, Austria

Keywords

Microdiffraction
Wood structure
Synchrotron
Crossfield pit
Microfibril angle
X-ray diffraction

Summary

The major part of the wood cell wall consists of parallel-aligned cellulose fibrils. Locally, pits connecting adjacent cell walls disturb the fibril arrangement. The local fibril orientation around these mechanically weak points is crucial for the mechanical stability of the cell. In some softwood species like spruce, the pit apertures at junctions of tracheids and cross-running ray parenchyma cells are elongated and slit-like. The pit orientation has often been assumed to directly reflect the fibril orientation. In this paper we use X-ray microdiffraction to determine the local microfibril angle (tilt angle versus the cell axis, MFA) in single tracheid walls of Norway spruce in the vicinity of pit apertures. The results from microdiffraction are compared with the pit orientation observed under the light microscope. Whereas a good correlation was found in thick-walled latewood cells from the stem and compression wood, large discrepancies occurred for thin-walled earlywood cells. A simple mechanical model that could explain the different situation in earlywood and latewood is presented.

Introduction

The orientation of the elementary cellulose fibrils reinforcing the wood cell wall has been a subject of growing interest in recent years. Particular attention has been attracted by the tilt angle of the cellulose fibrils with respect to the longitudinal cell axis (microfibril angle, MFA) that was found to influence the mechanical properties of wood (Haughton *et al.* 1968; Cave 1968, 1969; Salmén and de Ruvo 1985; Cave and Walker 1994; Reiterer *et al.* 1999) as well as shrinkage during drying (Meylan 1972). MFA was also discussed with respect to influences on stiffness and tensile strength of fibres and paper (Watson and Dadswell 1964; French *et al.* 2000; Wimmer *et al.* 2002).

Methods to measure MFA include wide angle x-ray scattering (Cave 1966; Boyd 1977; Evans 1999), small-angle x-ray scattering (Jakob *et al.* 1994, 1995, 1996; Reiterer *et al.* 1998; Lichtenegger *et al.* 1999), maximum extinction position using polarized light (Page 1969; El-Hosseiny and Page 1973; Leney 1981) and the inclination of small splits in the cell wall or iodine crystals on partially delignified cells (Senft and Bendtsen 1985). Wang *et al.* (2001) suggested an improvement of the iodine method which is based upon a modified ultrasonic treatment, using different metal salt solutions applied

before and during ultrasonic treatment. Another method refers to the measurement of the pit apertures, which is assumed to follow the MFA of the S2 layer of the secondary wall (Cockrell 1974; Donaldson 1991; Herman *et al.* 2000). Recently, confocal microscopy has also shown utility in the measurement of MFA through detection of polarized laser light intensity reflected from the fibre (Batchelor *et al.* 1997; Bergander *et al.* 2002).

The recently increased attention on MFA in wood has also encouraged researchers to compare different measuring methods (*e.g.*, Butterfield 1998; Huang *et al.* 1998; Anderson *et al.* 2000; Bergander *et al.* 2002). These approaches are important, as encountered discrepancies foster new research towards a better understanding of MFA in wood.

In the present paper, X-ray microdiffraction was applied on single cell walls to determine the orientation of elementary cellulose in longitudinal tracheids outside and inside of so-called crossfields, the latter formed at the conjunction of vertical tracheids with horizontally crossing ray parenchyma cells. Microdiffraction MFA was compared with the light microscopically determined inclination of pit apertures found in crossfields relative to the longitudinal axis. It was possible to perform both measurements on identical tracheids. Based

on mechanical and geometrical considerations, a model is suggested that might help to explain MFA discrepancies between earlywood and latewood encountered with different methods.

Material and Methods

Sample preparation

Wood samples were taken from a mature (about 90-year-old) Norway spruce (*Picea abies* L. [Karst.]) grown in the Wienerwald, Austria. Cubes with $1 \times 1 \times 1$ cm in size were cut from the juvenile (15–17th ring) and from the adult wood (70–75th ring) of a stem disk taken at breast height. An additional sample was cut from the bottom (abaxial) side of a primary branch that inserted at the bottom section of the crown. To ensure a selection with expressed differences, MFA was initially measured in each annual ring using position resolved small-angle X-ray scattering (scanning SAXS, Fratzl *et al.* 1997; Reiterer *et al.* 1998; Lichtenegger *et al.* 1998, 1999). This was done on 200 μm thick longitudinal (radial) sections cut from the cubes by means of a sliding microtome. The cubes were then infiltrated with polymethylmethacrylate and 10 μm thick sections were cut with a rotary microtome. The 10 μm section thickness corresponded to approximately half of the radial diameter of a spruce tracheid (Fig. 1a). Based on the initial scanning SAXS results, earlywood, latewood and compression wood samples were selected to represent a wide range of MFA for the X-ray microdiffraction (synchrotron) experiments. The thin-sections were placed on copper grids (3×3 mm) as used in electron microscopy. Polarized-light microscopy images were captured for the selection of characteristic crossfield regions.

X-ray microdiffraction

X-ray microdiffraction was carried out at the European Synchrotron radiation facility (ESRF) in Grenoble, France (Beamline ID 13, microfocus). Focusing of the beam to a spot diameter of 2 μm was achieved by using an ellipsoidal mirror and a glass capillary (Riekel *et al.* 1997). The wavelength of the beam was 0.96 \AA . A guard aperture (Pt-Ir, 10 μm in diameter) reduced diffuse scattering from the glass capillary and the diffraction patterns were recorded in transmission by a charge-coupled device (CCD) detector (Phontonic science, pixel resolution: $27.6 \times 27.6 \mu\text{m}^2$). A computer controlled stage allowed moving the sample through the beam in two orthogonal direc-

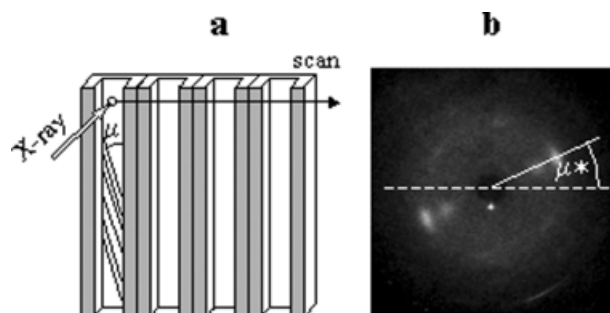


Fig. 1 (a) Longitudinal section through schematic tracheids. The microfibril angle in the radial walls is denoted by μ . For the microdiffraction measurement, a 2 μm thick X-ray beam is scanned across the cells perpendicular to the cell axis (arrow). (b) Typical diffraction pattern from a single cell wall: the meridional $110+1\bar{1}0$ and 020 reflections (indexing according to Gardner and Blackwell 1974) indicate the orientation μ^* of the cellulose fibrils as seen in projection.

tions, perpendicular to the beam. Beam position on the sample was exactly determined by means of an online video microscope, calibrated with a standard sample (kevlar cross). This allowed position-resolved scans across cells at a spatial resolution of 2 μm , corresponding to the diameter of the beam. Diffraction patterns were acquired within 20 s.

To determine the MFA near crossfield pits, radial sections were positioned perpendicular to the beam with the tracheids vertically aligned. Orientation of the cellulose fibrils was determined within and outside the crossfield regions of the same tracheid through several linear scans perpendicular to the cell axis (Fig. 1a). Since the 020 and $110+1\bar{1}0$ cellulose reflections (indices according to Gardner and Blackwell 1974) are known to occur in the plane perpendicular to the fibril axis (Preston 1934), the orientation of these reflections was used to determine the orientation of the fibrils (Fig. 1b). The orientation μ^* of the reflections with respect to the horizontal direction is equal to the microfibril angle μ , if diffraction patterns are recorded in the central part of the radial wall. Cellulose fibrils located at the tracheid corners are seen in projection and the angle μ^* determined by diffraction is smaller than the MFA μ following

$$\tan \mu^* = \tan \mu \sin \alpha \quad (1)$$

where α is the orientation of the part of cell wall under investigation with respect to the incident beam (Reiterer *et al.* 1998; Lichtenegger *et al.* 1999). For radial walls, $\alpha = 90^\circ$ and $\tan \mu^* = \tan \mu$, for tangential walls $\alpha = 0^\circ$ and therefore $\mu^* = 0^\circ$. For this reason, a linear scan perpendicular to the longitudinal cell axis resulted in a variation of observed angles between $\mu^*=0^\circ$ and $\mu^*=\mu$, where μ is the true microfibril angle. In principle, the experimental values μ^* must be corrected for the Ewald sphere curvature, in order to obtain correct values of μ , according to

$$\mu^*_{\text{corr}} = \arcsin(\sin \mu^* \sin \theta) \quad (\text{Lichtenegger } et al. 1998) \quad (2)$$

with 2θ being the scattering angle. In the present case with a wavelength of 0.96 \AA , the scattering angle for the 020 reflection was $2\theta=14.04^\circ$ and the correction yielded only small changes about 0.3° , which is within the experimental accuracy. Therefore, this effect was neglected and the values for μ^* were directly evaluated.

Pit aperture orientation

The polarized-light microscopy images captured for the selection of characteristic crossfield regions in the synchrotron were also used to determine the orientation of the pit apertures. The piceoid pit aperture angles in the crossfields with respect to the longitudinal axis of the tracheids were determined as shown, *e.g.*, by Herman *et al.* (1999).

Results

MFA in compression wood

Figure 2 shows results for the abaxial branch compression wood sample. The polarized light microscope image in Figure 2a shows elliptical-shaped crossfield pits in the upper half of the image. The scan was set close but outside the crossfield region. In Figure 2b the results from the microdiffraction experiment are seen. The orientation μ^* of the meridional 020 and $110+1\bar{1}0$ cellulose reflections with respect to the horizontal direction (compare Fig. 1b) was plotted versus the position perpendicu-

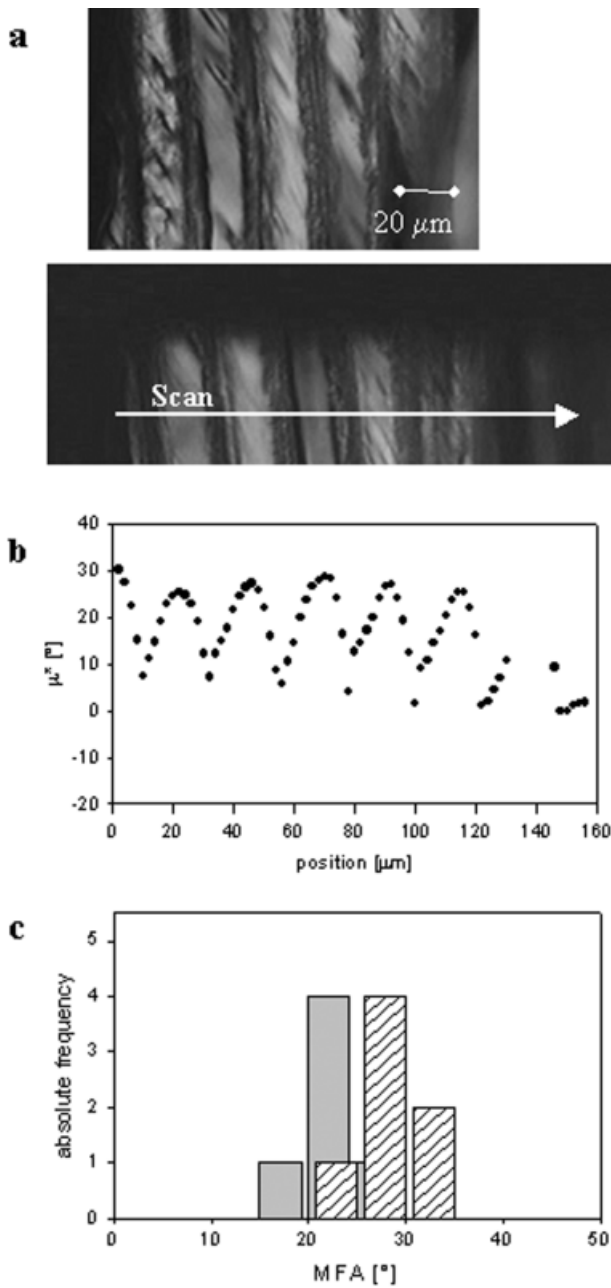


Fig. 2 Compression wood: abaxial side of a spruce branch. (a) Polarized light microscope image (on copper grid) of tracheids in a radial section. The slit-like crossfield pits are seen in the upper part, the lower part shows unpitted tracheid walls with drying fissures. The white arrow indicates the scanning positions of the microbeam across the cells. (b) Microdiffraction scan. Due to the tubular shaped tracheids, μ^* varied from 0° in the tangential walls to μ , the true microfibril angle, in the radial walls. The five peaks indicate a scan over five complete cells. The plot positions are vertically aligned with the micrograph. (c) Absolute frequency of local MFA (gray bars) and crossfield pit aperture angles (hatched bars). The height of the bars denotes the frequency of occurrence of angles in a given interval filled by the bar (the slight shift of the bars versus one another is for better visibility of overlapping results). One can see that the microdiffraction MFA values and results from pit angle measurements are in good agreement.

lar to the cell axis. Due to scanning over tangential as well as radial walls, the measured angle varied between 0° and μ (eq. 1). Therefore, the 5 peaks in Figure 2b correspond to the scan over 5 complete cells (Fig. 2a) and the amplitudes represent the microfibril angle in each of them. Figures 2a and b are on scale, which means the μ^*

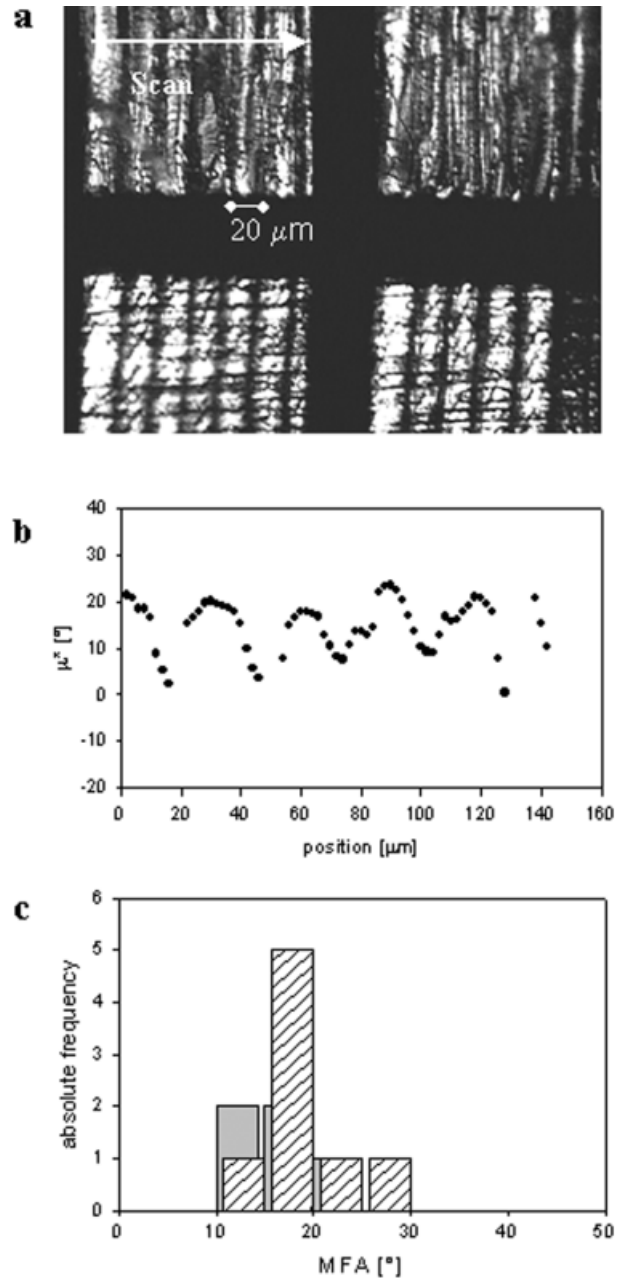


Fig. 3 Latewood with high MFA (20° as determined by SAXS). (a) Polarized light microscopy image (on copper grid) showing radially sectioned latewood tracheids; the microdiffraction scan was performed in an unpitted region (upper part, white arrow); crossfield pits are seen in the lower part of the image; the magnification is lower than in Figure 2, (a) and (b) are not on the same scale. (b) Local MFA in projection μ^* plotted versus position. μ^* varied between 0° and a maximum of 20° , giving a mean local fibril orientation of $16.3^\circ \pm 4.0^\circ$. (c) Absolute frequency of local MFA determined by microdiffraction (gray bars) and pit aperture orientation (hatched bars).

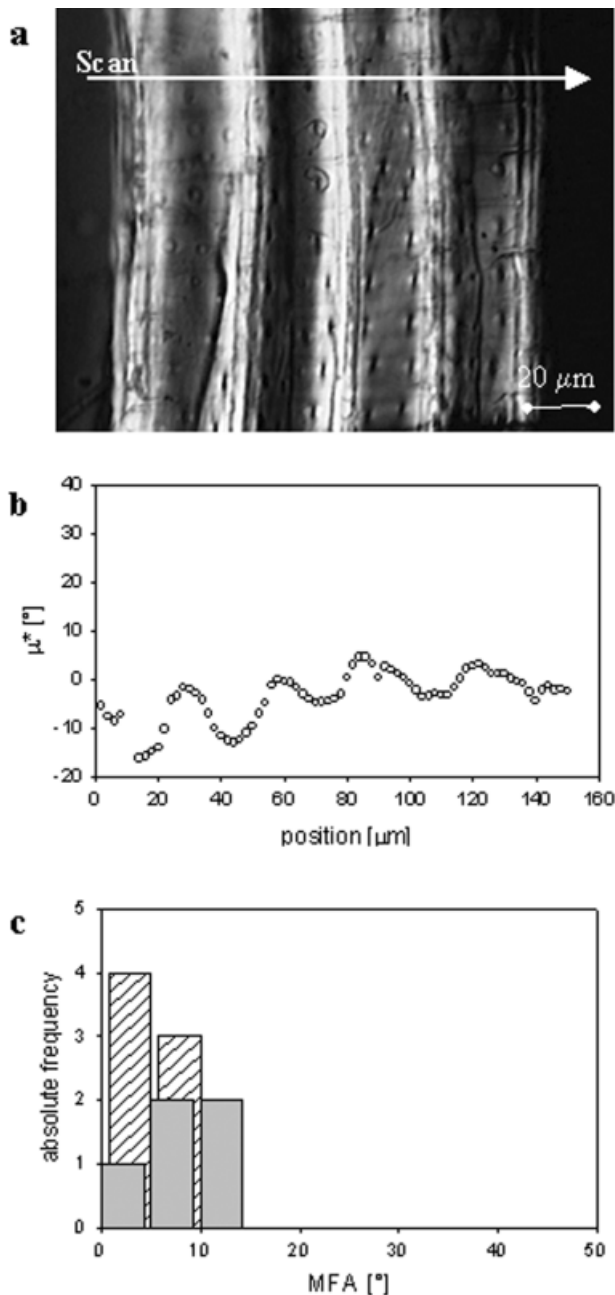


Fig. 4 Latewood with small MFA ($< 7^\circ$ as determined by SAXS). (a) Polarized light microscope image (on copper grid), radial section. The crossfield pits are almost vertically oriented. The white arrow indicates the region scanned with the microbeam. (b) The microdiffraction results show a small variation of μ^* giving a local MFA of $8.5^\circ \pm 2.7^\circ$. (c) Absolute frequency of local MFA (gray bars) and pit orientation (hatched bars).

values shown in Figure 2b can be directly lined up with their relative cell wall positions. The mean microfibril angle determined by microdiffraction was $22.9^\circ \pm 2.7^\circ$. The actual orientation of the pit apertures was deduced from the microscope image which gave a mean angle of $29.4^\circ \pm 2.3^\circ$, larger than obtained through microdiffraction. However, in Figure 2c absolute frequencies of microfibril angle values (grey bars) and pit orientation angles (hatched bars) still overlap.

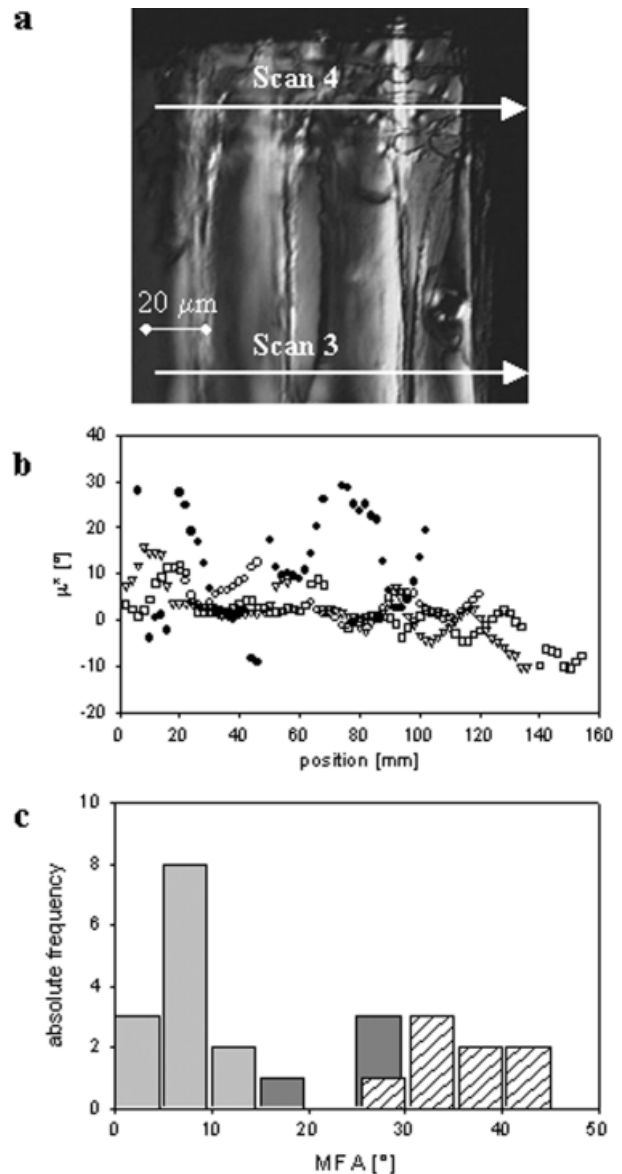


Fig. 5 Earlywood with small MFA ($< 7^\circ$ as determined by SAXS). (a) Radial section through earlywood tracheids (polarized light microscope image). The crossfield pit aperture angles are high, in contrast to the SAXS results. Microdiffraction scans were performed within the crossfield (scan 4) and outside (scans 1, 2, 3). Scans 1 and 2 were carried out further below scan 3 (not shown). (b) Results from microdiffraction scans: Scans 1, 2, 3 (outside pit region, open symbols) and scan 4 (right within pit region, full symbols). The fibril orientation within the crossfield ($24.5^\circ \pm 5.2^\circ$) differed considerably from that outside the crossfield ($7.7^\circ \pm 3.2^\circ$) (c) Absolute frequency of microdiffraction MFA (gray bars) and local pit orientations (hatched bars). The MFA values obtained by microdiffraction outside the pit region (light gray bars) are completely different from the pit angles (hatched bars). The microdiffraction MFA measured within crossfields (dark gray bars) comes closer to the pit angles, but is still lower.

MFA in latewood

In Figure 3 results from latewood samples with a mean MFA of 20° as determined with SAXS are shown. The upper half of the polarized light micrograph (Fig. 3a)

Table 1. Microfibril angles determined by scanning SAXS (mean over ca. 100 complete cells), X-ray microdiffraction (synchrotron) and crossfield pit aperture orientation of different samples. Mean values over the measured cells are given together with standard deviations

sample	MFA (SAXS laboratory)	MFA (microdiffraction, synchrotron)	pit angle
branch		22.9°±2.7°	29.4±2.3°
latewood, stem	20°	16.3°±4.0°	18.8±5.0°
latewood stem	<7°	8.5°±2.7°	5.0°±3.5°
earlywood, stem	<7°	7.7°±3.2°, 24.5°±5.2°*	35.8°±4.9°

* denotes results from a scan directly across the crossfield pits.

shows cell walls outside the crossfields; the lower half is crossfield region. The mean orientation of the pit apertures was 18.8°±5.0°, which agreed well with the MFA determined by SAXS. The results of the microdiffraction scan performed across several cells outside the crossfield region (as indicated in Fig. 3a) are shown in Figure 3b. Since the microscope image was only available at low magnification, the horizontal positions of measurements in Figure 3b do not line up with Figure 3a. In Figure 3c the absolute frequency of pit aperture angles (hatched bars) and microdiffraction MFA (grey bars) are shown. The obtained results widely overlap.

In Figure 4, results of a latewood sample with a microfibril angle < 7° (as pre-determined by scanning SAXS) are shown. The crossfield pit apertures are almost vertically oriented, with only a slight inclination versus the cell axis (5.0°±3.5°, Fig. 4a). Microdiffraction also yielded small angles (Fig. 4b), with a mean of 8.5°±2.7°. In Figure 4c the absolute frequencies of occurrence are plotted and the results clearly coincide (grey bars: local MFA, hatched bars: pit orientation).

MFA in earlywood

The earlywood samples showed a very different picture. The preceding SAXS measurements yielded a mean MFA < 7°, which disagreed with the visually measured pit aperture orientation as high as 35.8°±4.9° (Fig. 5c, hatched bars). For further clarification, microdiffraction scans were performed in and outside the pit region of identical tracheids. In Figure 5a positions of scans are indicated, scan 3 was set outside the pit region whereas scan 4 went right through crossfield pits. Scans 1 and 2 were performed below scan 3, also outside the crossfields (not visible in the image). The results of all scans are plotted in Figure 5b. Open symbols denote results from scans 1, 2 and 3 (outside crossfield region), full symbols results from scan 4 (inside crossfield region). Obvious differences existed in the orientation of cellulose fibrils: outside the crossfield region MFA were small with a mean value of 7.7°±3.2°. This is in good accordance with the previously determined SAXS data. In contrast, inside the crossfield region microdiffraction MFA were much larger (24.5°±5.2°). In Figure 5c the microdiffraction results (dark grey bars: measurement

in the pit region, light grey: outside the pit region) are compared with the results of the pit aperture angle measurements (hatched bars). The cellulose fibrils roughly follow the orientation of pit apertures in the crossfields, but the orientation outside the pit region of the same tracheid is very different. Table 1 summarizes the SAXS results, the microdiffraction on single cell walls and the pit angle measurements.

Discussion and Conclusions

X-ray microdiffraction experiments on single cell walls showed that the orientation of crossfield pit apertures and cellulose fibril orientation are not always in agreement. For compression wood taken from the lower side of a branch and for latewood of a stem-grown tree-ring, the orientation of the pit apertures corresponded sufficiently well with the mean microfibril angle measured by SAXS. Crossfield pit aperture orientation also corresponded with MFA of single cell walls measured by synchrotron X-ray microdiffraction. In earlywood, however, the mean MFA determined by SAXS was considerably smaller than the pit aperture angles. Further, fibril orientation in single tracheids inside and outside of a crossfield was different: inside the crossfield the fibrils roughly followed the pit aperture orientation, whereas outside the crossfields the fibril orientation corresponded with the mean MFA measured by SAXS.

Problems and restrictions with the determination of MFA in earlywood tracheids using the orientation of crossfield pits have been reported earlier. The use of crossfield pit apertures is generally restricted to species with piceoid or distinct pinoid crossfield apertures because these species give a clear indication of the angle due to the elliptical shape of their aperture in the S2 layer of the tracheid wall (Markstrom *et al.* 1983; Donaldson 1991). In a comparative study by Huang *et al.* (1998) results from iodine staining, pit aperture orientation and X-ray diffraction measurements correlated well in latewood, but low correlation was found in earlywood. The discrepancies were particularly large in softwoods like spruce. Khalili *et al.* (2001) used soft rot fungi to remove the matrix between the fibrils and found that the resulting cavities indicating the fibril orientation were more or less parallel to the pit apertures in latewood, but not in earlywood.

Several issues related to the question of why differences were encountered in earlywood but not in latewood could be discussed. Wang *et al.* (2001) observed a change in MFA at different depths in the S2 layer. The crossing fibrillar arrangements of the S1 or S3 layer, which are also composed of several layers (Wardrop 1964), were visible, displaying a much larger angle than in the S2 layer (Abe *et al.* 1992). The fairly wide range of fibril angles prevalent in the multiple lamellae nature of a cell wall is expressed more in the earlywood than in the latewood and might account for the higher variability or encountered differences across methods.

The question of what determines the orientation of a slit-like aperture at a junction of cross-running cells (longitudinal tracheids crossing ray parenchyma cells) with presumably different fibril orientation on either side, has led the authors to another explanation, which may be found in the minimization of moment and therefore minimization of failure probability by optimum orientation of the slit.

For simplification, we assume a single tracheid wall consisting of only an S2 layer with parallel fibrils oriented at an angle μ_T versus the tracheid axis (Fig. 6a). Adjacent to the tracheid wall we consider a single wall of a ray parenchyma cell with a fibril orientation of μ_P versus the long axis of the parenchyma cell (perpendicular to the tracheid axis, see Fig. 6b). This implies that the difference between the fibril orientations is

$$\delta = \frac{\pi}{2} - \mu_P - \mu_T \quad (3)$$

Note that all angles are counted in radian. It is logical to assume that a slit-like aperture connecting the two cells will run parallel to the cellulose fibrils. This is, however, impossible to achieve for both the tracheid and the parenchyma cell, except in the special case where $\delta = 0$. To fit the aperture through both the cells it is, therefore, necessary to assume a certain rotation of the aperture with respect to the overall direction defined by the microfibril angle. In our model, we assume that this rotation is achieved by shearing the cell walls of both cells as sketched in Figure 6. This results approximately in a moment

$$M_T = G (\rho - \mu_T) D_T D_P d_T \quad (4)$$

acting on the pit in the tracheid. G is the elastic shear modulus of the cell wall material and $D_T D_P d_T$ is the sheared volume around the pit, with D_T and D_P being the width of the tracheid and the parenchyma cell walls, respectively, and d_T being the thickness of the tracheid wall. Similarly one gets

$$M_P = G \left(\frac{\pi}{2} - \rho - \mu_P \right) D_T D_P d_P \quad (5)$$

for the moment acting on the pit in the ray parenchyma, where d_P is the thickness of the parenchyma cell wall. (For simplicity, the shear modulus G is assumed to be

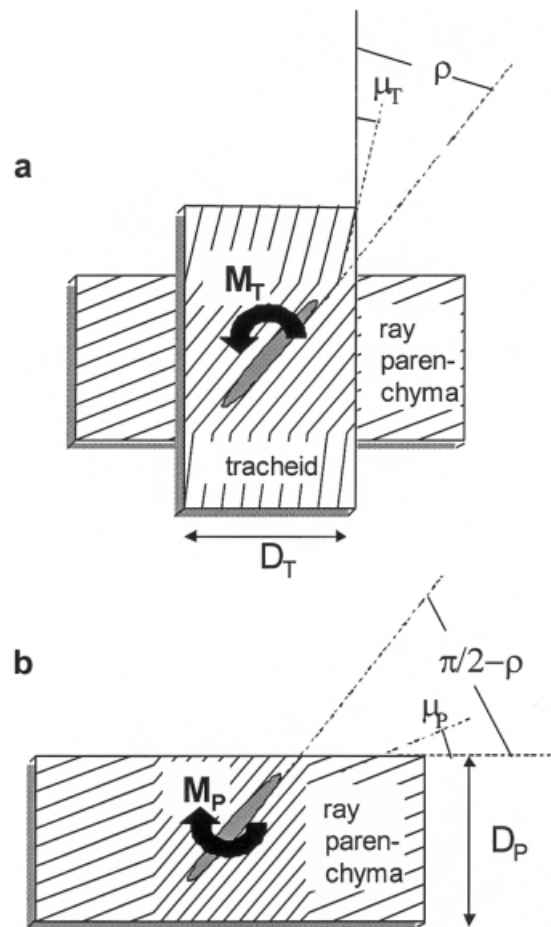


Fig. 6. Pit (half-bordered) connecting a longitudinal tracheid to a ray parenchyma. The overall microfibril angles of the corresponding cell walls are μ_T and μ_P , respectively. The angle of the pit aperture with respect to the tracheid axis is ρ . The diameters of tracheid and ray parenchyma are D_T and D_P , respectively, the thickness of their cell walls, d_T and d_P (not shown in graph). M_T (see a) and M_P (see b) are the moments acting on the tissue around the pit due to the distortions necessary to get the same orientation of cellulose fibrils around the pit in both types of cells.

the same for the tracheid and the parenchyma cell walls.) Mechanical equilibrium requires $M_T = M_P$, or

$$\frac{\pi}{2} - \rho - \mu_P = (\rho - \mu_T) \frac{d_T}{d_P} \quad (6)$$

This can easily be rewritten as

$$\rho = \frac{\mu_T d_T + (\pi/2 - \mu_P) d_P}{d_T + d_P}$$

and, with the use of (3), be further simplified to give

$$\rho = \mu_T + \frac{d_P}{d_T + d_P} \delta \quad (7)$$

This simple expression predicts that the angle of the pit aperture is the same as the microfibril angle in the tracheids if one of the following conditions is fulfilled:

1. $\delta = 0$, that is, the microfibril angles of the tracheid and of the ray parenchyma add up to 90° , corresponding to a parallel alignment of cellulose fibrils in adjacent cell walls;
2. the cell wall of the ray parenchyma is much thinner than the wall of the tracheid.

Condition 1 may be fulfilled in special cases, but this would rather be accidental. In the case of thick latewood tracheids, condition 2 would come into play and the influence of the parenchyma cell wall could be neglected. In this case, the pit angle would be close to the microfibril angle in the tracheid. The wall of earlywood cells being much thinner, however, it follows that the influence of the parenchyma cell wall becomes crucial and the microfibril angle would differ considerably from the pit angle in earlywood. This could explain the relatively good correlation of mean microfibril angles with pit aperture orientation found in latewood and compression wood and the large discrepancies in earlywood.

Acknowledgements

This work was in part supported by the Fonds zur Förderung der Wissenschaftlichen Forschung (FWF, project P14331-PHY). R. Wimmer was supported by the Austrian Programme for Advanced Research and Technology (APART), of the Austrian Academy of Science.

References

- Abe, H., J. Ohtani and K. Fukazawa. 1992. Microfibrillar orientation of the innermost surface of conifer tracheid wall. *IAWA Bull.* 13, 411–417.
- Anderson, S., R. Serimaa, M. Torkkeli, T. Paakkari, P. Saranpää, P. and E. Personen. 2000. Microfibril angle of Norway spruce [*Picea abies* (L.) Karst.] compression wood: Comparison of measuring technique. *J. Wood Sci.* 46, 343–349.
- Batchelor, W.J., A.B. Conn and I.H. Parker. 1997. Measuring the fibril angle of fibres using confocal microscopy. *Appita J.* 50, 377–380.
- Bergander, A., J. Brändström, G. Daniel and L. Salmén. 2002. Fibril angle variability in earlywood of Norway spruce using soft rot cavities and polarization confocal microscopy. *J. Wood Sci.* (under review)
- Boyd, J.D. 1977. Relationship between fibre morphology and shrinkage of wood. *Wood Sci. Technol.* 11, 3–22.
- Butterfield, B.G. 1998. Microfibril Angle in Wood, Proceedings of the IAWA/IUFRO International Workshop on the Significance of Microfibril Angle to Wood Quality, Westport, New Zealand, November 1997.
- Cave, I.D. 1966. X-ray measurement of microfibril angle. *For. Prod. J.* 44, 37–42.
- Cave, I.D. 1968. The anisotropic elasticity of the plant cell wall. *Wood Sci. Technol.* 2, 268–278.
- Cave, I.D. 1969. The longitudinal Young's modulus of *Pinus radiata*. *Wood Sci. Technol.* 3, 40–48.
- Cave, I.D. and J.C.F. Walker. 1994. Stiffness of wood in fast-grown plantation softwoods: The influence of microfibril angle. *For. Prod. Journal* 44, 43–48.
- Cockrell, R.A. 1974. A comparison of latewood pits, fibril orientation, and shrinkage of normal and compression wood of Giant Sequoia. *Wood Sci. Technol.* 8, 197–206.
- Donaldson, L.A. 1991. The use of pit apertures as windows to measure microfibril angle in chemical pulp fibres. *Wood Fiber Sci.* 23, 290–295.
- Evans, R. 1999. A variance approach to the X-ray diffractometry estimation of microfibril angle in wood. *Appita J.* 52, 283–294.
- El-Hosseiny, F. and D.H. Page. 1973. The measurement of fibril angle of wood fibers using polarized light. *Wood Fiber* 5, 208–214.
- Fratzl, P., H.F. Jakob, S. Rinnerthaler, P. Roschger and K. Klaushofer. 1997. Position resolved small-angle X-ray scattering of complex biological materials. *J. Appl. Cryst.* 30, 765–769.
- French, J., A.B. Conn, W.J. Batchelor and I.H. Parker. 2000. The effect of fibre fibril angle on some handsheet mechanical properties. *Appita J.* 53, 210–226.
- Gardner, K.H. and J. Blackwell. 1974. The Structure of Native Cellulose. John Wiley & Sons, New York. pp. 1975–2001.
- Haughton, P.M., D.B. Sellen and R.D. Preston. 1968. Dynamic mechanical properties of the cell wall of *Nitella opaca*. *J. Exp. Bot.* 19, 1–12.
- Herman, M., P. Dutilleul and T. Avella-Shaw. 1999. Growth rate effects on intra-ring and inter-ring trajectories of microfibril angle in Norway spruce (*Picea abies*). *IAWA J.* 20, 3–21.
- Herman, M., P. Dutilleul and T. Avella-Shaw. 2000. Growth rate effects on intra-ring and inter-ring variations of the morphology and ultrastructure of the tracheid in Norway spruces: Influence on paper indices. *In: Proceedings of a COST Action E20 workshop: Fibre Wall & Microfibril Angle.* 11th–13th May 2000, Athens, Greece. pp. 23–29.
- Huang, C.L., N.P. Kutscha, G.J. Leaf and R.A. Megraw. 1998. Comparison of microfibril measurement techniques. *In: Microfibril Angle in Wood, Proceedings of the IAWA/IUFRO International Workshop on the Significance of Microfibril Angle to Wood Quality.* Westport, New Zealand, November 1997. pp. 177–205.
- Jakob, H.F., S.E. Tschegg and P. Fratzl. 1994. Size and arrangement of elementary cellulose fibrils in wood cells: A small angle X-ray scattering study of *Picea abies*. *J. Struct. Biol.* 113, 13–22.
- Jakob, H.F., D. Fengel, S.E. Tschegg and P. Fratzl. 1995. The elementary cellulose fibril in *Picea abies*: Comparison of transmission electron microscopy, small-angle X-ray, and wide-angle X-ray scattering results. *Macromolecules* 26, 8782–8787.
- Jakob, H.F., S.E. Tschegg and P. Fratzl. 1996. Hydration dependence of the wood-cell wall structure in *Picea abies*. A small-angle X-ray scattering study. *Macromolecules* 29, 8435–8440.
- Khalili, S., T. Nilsson and G. Daniel. 2001. The use of soft rot fungi for determining the microfibrillar orientation in the S2 layer of pine tracheids. *Holz Roh- Werkst.* 58, 439–447.
- Leney, L. 1981. A technique for measuring fibril angle using polarized light. *Wood Fiber* 13, 13–16.
- Lichtenegger, H., A. Reiterer, S. Tschegg and P. Fratzl. 1998. Determination of spiral angles of elementary fibrils in the wood cell wall: Comparison of small-angle X-ray scattering and wide-angle X-ray diffraction. *In: Microfibril Angle in Wood, Proceedings of the IAWA/IUFRO International Workshop on the Significance of Microfibril Angle to Wood Quality.* Westport, New Zealand, November 1997. pp. 140–156.
- Lichtenegger, H., A. Reiterer, S.E. Stanzl-Tschegg and P. Fratzl. 1999. Variation of cellulose microfibril angles in softwoods and hardwoods: A possible strategy of mechanical optimization. *J. Struct. Biol.* 128, 257–269.
- Markstrom, D.C., H.E. Troxell and C.E. Boldt. 1983. Wood properties of immature ponderosa pine after thinning. *For. Prod. J.* 33, 33–36.

- Meylan, B.A. 1972. The influence of microfibril angle on the longitudinal shrinkage-moisture content relationship. *Wood Sci. Technol.* 6, 293–301.
- Page, D.H. 1969. A method for determining fibrillar angle in wood tracheids. *J. Roy. Microsc. Soc.* 90, 137–143.
- Preston, R.D. 1934. The organization of the cell wall of the conifer tracheid. *Phil. Trans.* 224, 131–174.
- Reiterer, A., H.F. Jakob, S.E. Stanzl-Tschegg and P. Fratzl. 1998. Spiral angle of elementary cellulose fibrils in cell walls of *Picea abies* determined by small-angle X-ray scattering. *Wood Sci. Technol.* 32, 335–345.
- Reiterer, A., H. Lichtenegger, S. Tschegg and P. Fratzl. 1999. Experimental evidence for a mechanical function of the cellulose microfibril angle in wood cell walls. *Philosophical Magazine A* 79(9), 2173–2184.
- Riekkel, C., A. Cedola, F. Heidelbach and K. Wagner. 1997. Microdiffraction experiments on single polymeric fibers by synchrotron radiation. *Macromolecules* 30(4), 1033–1037.
- Salmén, L. and A. de Ruvo. 1985. A model for the prediction of fiber elasticity. *Wood Fiber Sci.* 17, 336–350.
- Senft, J.F. and B.A. Bendtsen. 1985. Measuring microfibrillar angles using light microscopy. *Wood Fiber Sci.* 17, 564–567.
- Wang, H.H., J.G. Drummond, S.M. Reath, K. Hunt and P.A. Watson. 2001. An improved fibril angle measurement method for wood fibres. *Wood Sci. Technol.* 23, 493–503.
- Wardrop, A.B. 1964. The structure and formation of cell wall in xylem. *In: The Formation of Wood in Forest Trees*. Ed. M.H. Zimmermann. Academic Press, New York. pp. 87–134.
- Watson, A.J. and H.E. Dadswell. 1964. Influence on fibre morphology on paper properties. 4. Micellar spiral angle. *Appita* 17, 151–156.
- Wimmer, R., G.M. Downes, R. Evans, G. Rasmussen and J. French, 2002. Direct effects of wood characteristics on pulp and handsheet properties of *Eucalyptus globulus*. *Holzforchung* 56, 244–252.

Received September 6th 2001

Helga C. Lichtenegger¹⁾
 Department of Chemistry and Biochemistry
 University of California Santa Barbara
 Santa Barbara CA 93106
 USA
 e-mail: lichtenegger@chem.ucsb.edu

Martin Müller
 Institute for Experimental and Applied Physics
 University of Kiel
 D-24098
 Germany

Rupert Wimmer
 Institute for Botany
 University for Agricultural Sciences
 Gregor-Mendel-Strasse 33
 A-1180 Wien
 Austria

Peter Fratzl
 Erich Schmid Institute for Materials Science
 Austrian Academy of Sciences and University of Leoben
 Jahnstrasse 12
 A-8700 Leoben
 Austria

¹⁾ Corresponding author